Applied Chemical Engineering (2025) Volume 8 Issue 3 ISSN: 2578-2010 (O)
doi: 10.59429/ace.v8i3.5750

ORIGINAL RESEARCH ARTICLE

Eco-friendly hydrogel based on carboxymethylcellulose poly (acrylic acid-co-hydroxyethyl acrylamide) (CMC-AAC-co-HEAM) for sustainable removal of Pb (II) ions from contaminated water

Ayaa Ahmed Shihab[1*], Layth S. Jasim[2]

[1] *Department of Chemistry, College of science, Lebanese university, Beirut, 146573,Lebanon*

[2] *Department of Chemistry, College of Education, University of Al-Qadisiyah, Diwaniyah, 58002, Iraq*

***Corresponding author:** Layth S. Jasim; layth.alhayder@qu.edu.iq

ABSTRACT

A hydrogel based on carboxymethylcellulose poly(acrylic acid-co-hydroxyethyl acrylamide) (CMC-AAC-co-HEAM) was synthesized via free radical polymerization and employed as an efficient adsorbent for the removal of Pb(II) ions from aqueous solutions. The influence of critical parameters, including adsorbent dosage, contact time, pH, ionic strength, and temperature, was systematically evaluated. Adsorption equilibrium was attained within 120 minutes, with a maximum uptake capacity of 39.8 mg/g. Kinetic studies demonstrated that the adsorption process was best described by the pseudo-second-order model, while isotherm analysis indicated favorable fitting to the Freundlich model, confirming multilayer adsorption on a heterogeneous surface. Thermodynamic investigations revealed that the adsorption was feasible, spontaneous, and endothermic, with negative ΔG values and a positive ΔH. Furthermore, the functional groups of the hydrogel, primarily carboxyl and hydroxyl moieties, played a central role in Pb(II) binding through electrostatic attraction and complexation. These results highlight the potential of CMC-AAC-co-HEAM hydrogel as a cost-effective and environmentally sustainable material for heavy metal remediation.

Keywords: Adsorption; Pb(II); CMC-AAC-co-HEAM; kinetics; isotherms; thermodynamics

ARTICLE INFO

3.Received: 24 August 2025
4.Accepted: 12 September 2025
Available online: 24 September 2025

Graphical Abstract

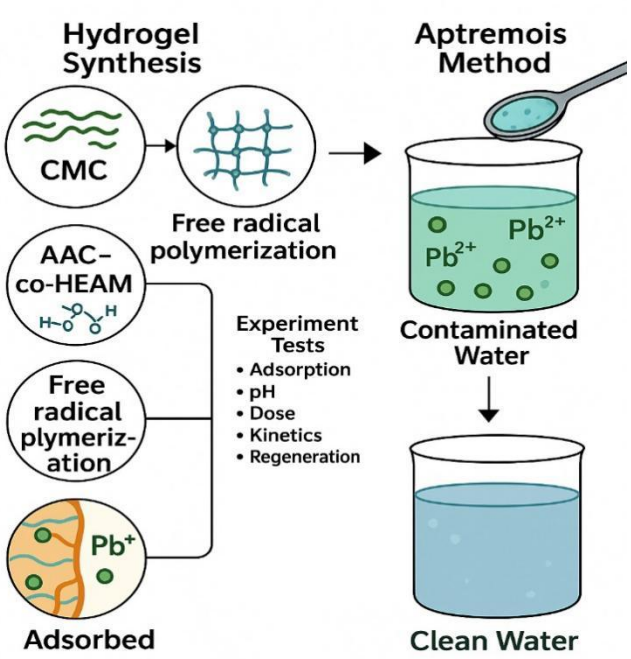

1.Introduction

Water contamination by heavy metals, particularly lead (Pb), has emerged as a critical environmental threat in the era of rapid industrialization and urban expansion. Lead enters aquatic systems through industrial effluents, corroded plumbing, and agricultural runoff, posing severe risks to human health and aquatic ecosystems [1]. Owing to its bioaccumulative properties and strong association with neurological, cardiovascular, and developmental disorders, the removal of Pb(II) from water has become a global priority [2]. Among the available treatment techniques, adsorption is recognized as one of the most efficient, cost-effective, and eco-friendly strategies [3-5]. This approach relies on the interaction of Pb(II) ions with the active surface sites of an adsorbent, with its efficiency largely governed by surface chemistry, solution pH, ionic competition, and temperature [6]. In recent years, extensive efforts have been devoted to designing sustainable adsorbents, particularly those derived from biopolymers. Materials such as chitosan, bentonite clay, rice husk, and other agricultural by-products have been investigated, with their adsorption capacity enhanced through cross-linking, functionalization, and hydrogel formation. These modifications improve selectivity and affinity toward Pb [7](II) ions, enabling better performance under diverse environmental conditions [1,8-10]. Parameters such as pH and temperature have been consistently reported as key factors influencing adsorption efficiency. To further advance this field, novel hydrogel hydrogels have been engineered with improved surface properties and stability [11,12]. In this study, a hydrogel based on carboxymethylcellulose poly(acrylic acid-co-hydroxyethyl acrylamide) (CMC-AAC-co-HEAM) was synthesized and applied for Pb(II) removal from aqueous media. The adsorption performance of this hydrogel was systematically investigated through kinetic, isothermal, and thermodynamic analyses, in addition to evaluating the effects of pH and ionic strength. By utilizing a biopolymer-based hydrogel with tailored functional groups, this work contributes to the development of cost-effective, environmentally sustainable solutions for heavy metal remediation. The synthesized hydrogel's maximum adsorption capacity of 39.8 mg/g compares to other eco-friendly adsorbents for Pb(II) removal, such as SA-g-P(FA-AA)/GO hydrogel (22.371 mg/g) [13] and rice husk nano adsorbent (16.26 mg/g) [14].

2. Experimental section

2.1. Materials

Lead nitrate ($Pb(NO_3)_2$) of analytical grade was purchased from Merck (Seoul, Republic of Korea). Carboxymethylcellulose (CMC), acrylic acid (AA, ≥99%), and hydroxyethyl acrylamide (HEAM, ≥98%) were obtained from Sigma-Aldrich (Germany). N,N'-methylenebisacrylamide (MBA, 99.5%) was supplied by Aladdin, while potassium persulfate (KPS, ≥98.5%) was used as a radical initiator. All chemicals were of high purity and used without further purification. Distilled water was employed throughout the study for the preparation of stock and working solutions.

2.2. Preparation of CMC-AAC-co-HEAM hydrogel

The hydrogel (CMC-AAC-co-HEAM) was prepared by dissolving carboxymethyl cellulose powder (1g) in deionized water (50mL) using a magnetic stirrer at 120 rpm for 30 minutes until complete dissolution occurred. This process was conducted in a 250mL three-necked round-bottom flask equipped with a condenser, thermometer, and nitrogen line while maintaining continuous stirring at 50°C. Hydroxyethyl acrylamide (4mL) was added to the aqueous carboxymethyl cellulose solution until homogenization was achieved, followed by the gradual addition of acrylic acid (4mL) at 25°C. MBA (0.01g) dissolved in deionized water (2mL) was slowly incorporated into the above solution with continuous stirring for 5 minutes. Subsequently, KPS (0.01g) dissolved in deionized water (2mL) was added to the carboxymethyl cellulose solution to generate free radicals. The mixture was then placed in a water bath at 70°C for three hours to complete the polymerization reaction. The resulting samples were washed with deionized water to

remove unreacted components and reagents, then dried in an oven at 60°C for 48 hours. The dried samples were ground and sieved for further analysis. **Figure 1** illustrates the hydrogel preparation steps, while Scheme (2-1) demonstrates the preparation mechanism of the hydrogel (CMC-AAC-co-HEAM).

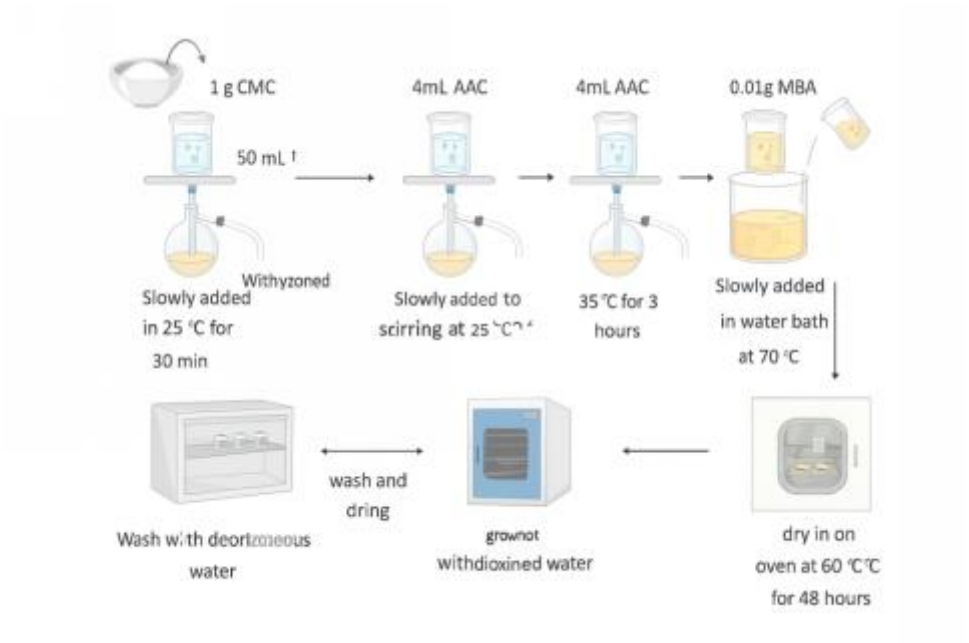

Figure 1. SA-g-P (AAc-CA) GO hydrogel synthesis

2.3. Characterization of CMC-AAC-co-HEAM hydrogel

The structural and surface properties of the synthesized CMC-AAC-co-HEAM hydrogel were characterized before and after Pb(II) adsorption. Fourier-transform infrared (FTIR) spectra were recorded in the range of 400–4000 cm^{-1} using a Shimadzu 8400S spectrophotometer to identify functional groups and confirm the interaction with Pb(II) ions [3]. The surface morphology was examined by field emission scanning electron microscopy (FESEM, MIRA3 TESCAN, 10 kV), while the elemental composition was determined using energy-dispersive X-ray spectroscopy (EDS, S-4800, Hitachi Corporation, Japan). In addition, powder X-ray diffraction (XRD) patterns were obtained on a Philips/PANalytical X'Pert MRD diffractometer equipped with Cu Kα radiation (λ = 0.1540 nm) over a 2θ range of 10–80°, providing insights into the crystalline structure of the hydrogel [15].

3. Results and discussion

3.1. Characterization of adsorbent

3.1.1. FTIR analysis

The FTIR spectra of the CMC-AAC-co-HEAM hydrogel before and after Pb(II) adsorption are presented in **Figure 1**. In both spectra, broad absorption bands observed between 3550 and 3100 cm^{-1} are attributed to –OH stretching vibrations, confirming the presence of hydroxyl groups originating from carboxymethylcellulose and acrylic acid units [16-18]. The peaks detected around 2921–2925 cm^{-1} correspond to –CH stretching vibrations of methyl and methylene groups. After Pb(II) adsorption, the –OH stretching band exhibited a shift to a higher wavenumber at approximately 3387 cm^{-1}, accompanied by a reduction in intensity, suggesting hydrogen bonding and electrostatic interactions between Pb(II) ions and the hydrogel matrix. Additional characteristic peaks were observed at 1045–1058 cm^{-1} and 1630–1641 cm^{-1}, corresponding to C–O and C=O stretching vibrations of hydroxyl and carboxyl functional groups, respectively. The noticeable shifts in these peaks after adsorption confirm the involvement of oxygen-

containing groups in the binding of Pb(II). These findings indicate that the adsorption mechanism primarily occurs through ion exchange, surface complexation via oxygen donor groups, and secondary interactions such as electrostatic attraction and van der Waals forces. [1-3,12]

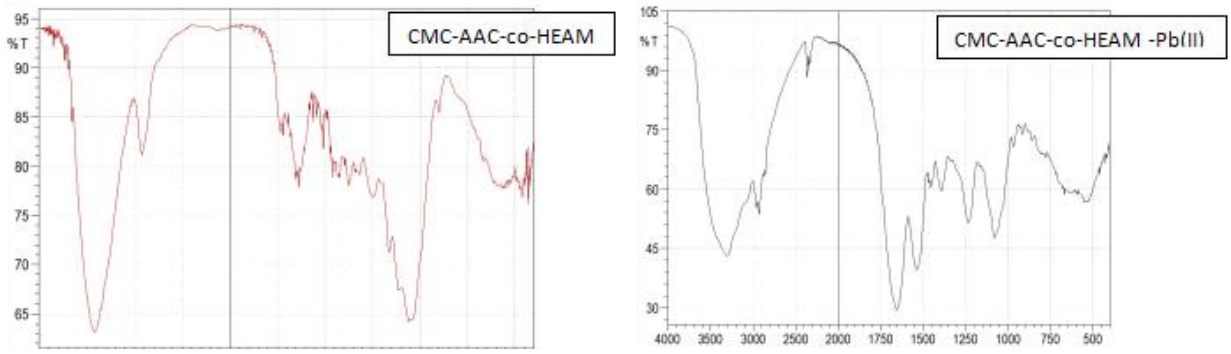

Figure 2. FTIR of CMC-AAC-co-HEAM hydrogel: a- before adsorption and b- after adsorption Pb(II) ions

3.1.2. XRD analysis

The crystalline nature of the synthesized CMC-AAC-co-HEAM hydrogel was investigated using X-ray diffraction (XRD), and the results are presented in **Figure 2**. The diffraction pattern displayed two broad peaks at 2θ = 19.73° and 39.3°, which are characteristic of semi-crystalline polymeric hydrogels. The peak at 19.73° corresponds to a hydrated crystalline structure, while the broad reflection at 39.3° is attributed to the amorphous phase of the material. The presence of these peaks confirms the coexistence of both crystalline and amorphous domains, indicating that the hydrogel possesses a predominantly amorphous structure with partial ordering [12,19].

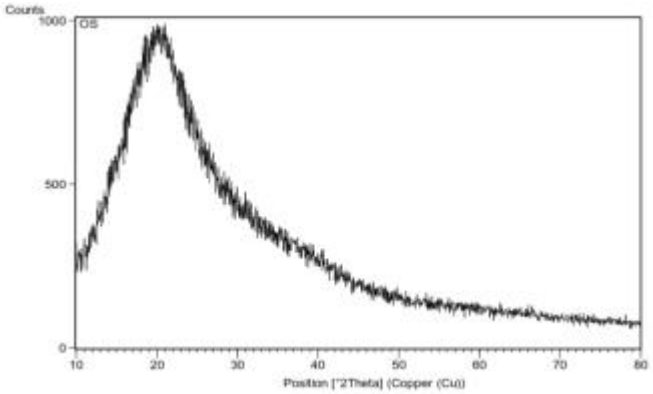

Figure 3. XRD pattern of the CMC-AAC-co-HEAM hydrogel

Table 1. XRD results of the CMC-AAC-co-HEAM hydrogel

Pos. [°2θ]	Height [cts]	FWHM Left [°2θ]	d-spacing (Å)	Rel. Int. [%]
19.73	298	8	4.4967	100
39.3	62	8	2.2921	20.83

Table 1 summarizes the XRD results, showing a d-spacing of 4.4967 Å at 19.73° with the highest relative intensity (100%), and a secondary peak at 39.3° with a d-spacing of 2.2921 Å and relative intensity of 20.83%. These findings suggest that the hydrogel framework is primarily amorphous, which enhances its flexibility and accessibility of functional groups, thereby facilitating Pb(II) ion diffusion and adsorption.

3.1.3. SEM-EDS characterization

The morphology of the CMC-AAC-co-HEAM hydrogel before and after Pb(II) adsorption was examined using SEM (**Figure 3**). Prior to adsorption, the hydrogel displayed a loose and porous network with interconnected pores, which is advantageous for the diffusion and trapping of metal ions. After Pb(II) exposure, the surface became less porous and was decorated with fine particles, indicating the successful attachment of Pb(II) ions onto the hydrogel matrix. To confirm the adsorption process, energy-dispersive X-ray spectroscopy (EDX) was employed. The analysis revealed the presence of carbon (38.54 wt%), oxygen (49.04 wt%), and a minor fraction of silicon (2.42 wt%), consistent with the organic–polymeric backbone of the material. After adsorption, a distinct Pb signal was observed, accounting for 10.00 wt%, providing direct evidence of Pb(II) ion immobilization on the hydrogel surface. The reduction in the relative percentages of carbon and oxygen highlights their involvement in Pb(II) binding through oxygenated functional groups. These results collectively confirm that the adsorption mechanism occurs via the interaction of Pb(II) ions with carboxyl and hydroxyl groups distributed across the hydrogel matrix, in addition to surface deposition [12,20,21].

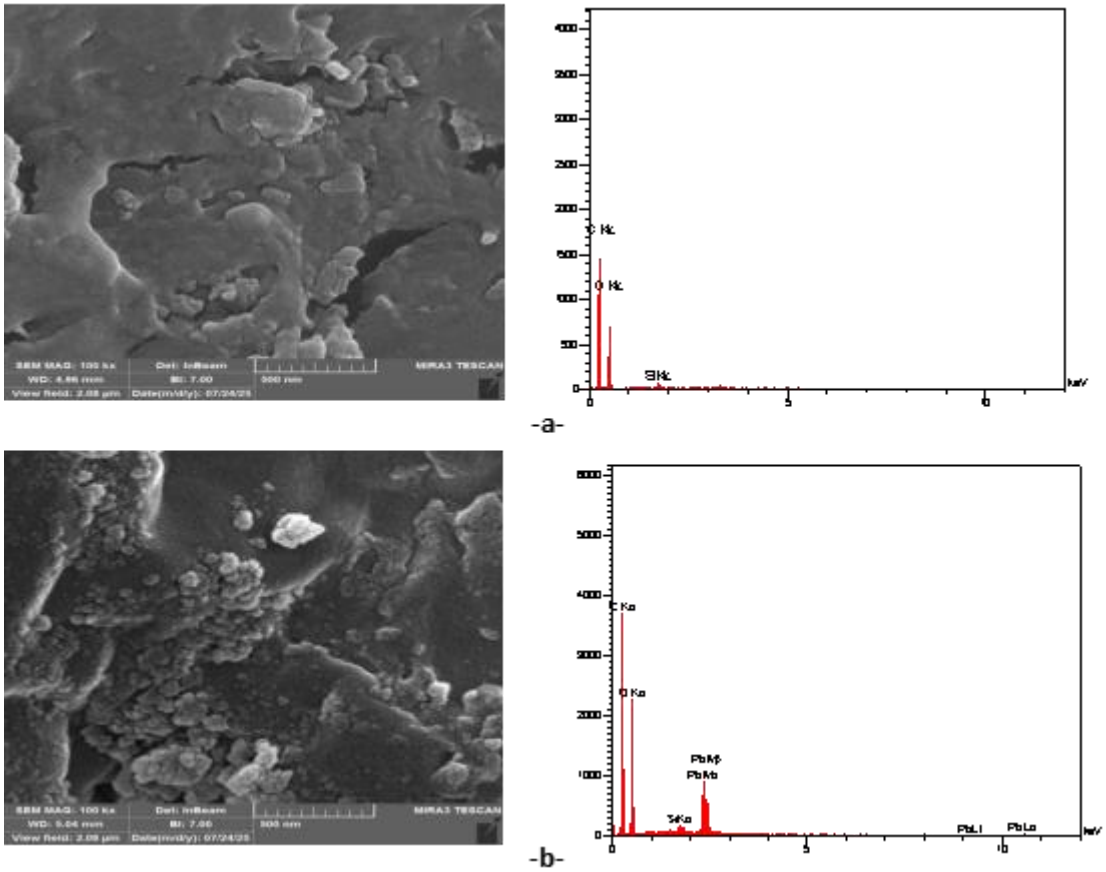

Figure 4. FE-SEM and EDS of CMC-AAC-co-HEAM hydrogel a. after, and b.before adsorption.

3.1.4. TGA- DTA analysis

Thermogravimetric analysis (TGA) and differential thermogravimetric (DTG) studies were performed to evaluate the thermal stability of the CMC-AAC-co-HEAM hydrogel under a nitrogen atmosphere in the range of 50–790 °C (**Figure 4**). The decomposition occurred in four main stages. The first stage, between 50 and 140 °C, showed a weight loss of 8.35%, which is attributed to the evaporation of physically adsorbed and bound water molecules. The second stage, from 140 to 280 °C, exhibited the most significant weight

reduction (33.88%), corresponding to the decomposition of labile functional groups and the onset of polymer backbone cleavage. The third stage, occurring between 280 and 450 °C, accounted for a 29.89% loss, associated with intramolecular reactions such as anhydration, esterification, and breakdown of polymer chains. The final stage, from 450 to 790 °C, resulted in a further 25.54% weight loss, representing the degradation of the remaining carbonaceous structures. At the end of the analysis, the hydrogel exhibited a total weight loss of 97.66%, confirming its predominantly organic composition. These results indicate that the CMC-AAC-co-HEAM hydrogel maintains good stability up to approximately 200 °C, while higher temperatures trigger progressive decomposition of the crosslinked polymer network [22].

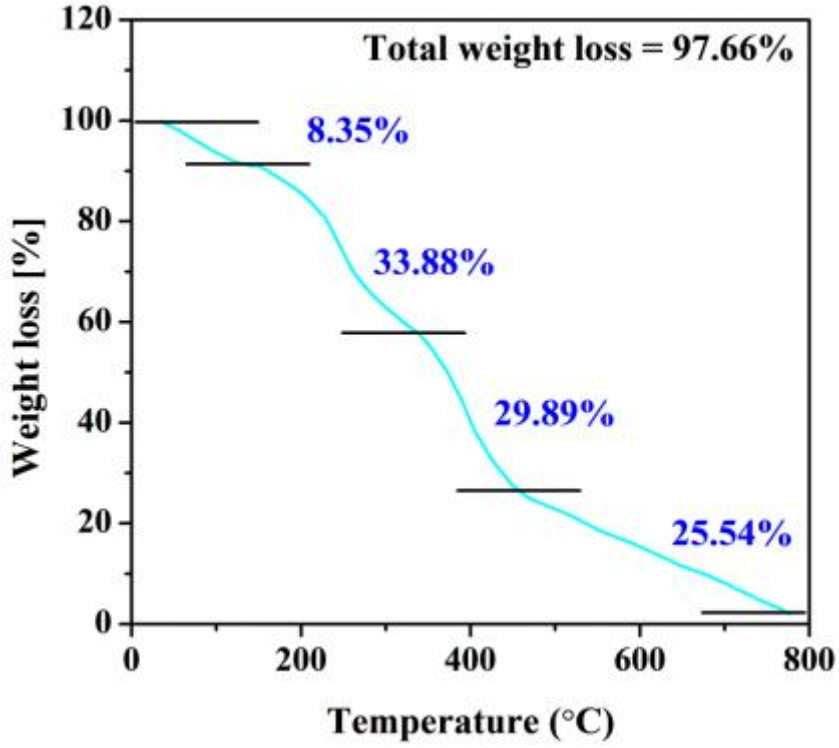

Figure. 5. Thermogravimetric (TGA/DTG) curve of the CMC-AAC-co-HEAM hydrogel.

3.2. Effects of adsorbent dosage

The influence of CMC-AAC-co-HEAM hydrogel dosage on Pb(II) adsorption is illustrated in **Figure 5**. The results demonstrate that increasing the adsorbent dosage enhances the removal efficiency (R%) but leads to a reduction in adsorption capacity (q_e). At lower dosages (e.g., 0.04 g/L), the available adsorption sites are rapidly saturated with Pb(II) ions, resulting in higher q_e values. However, as the dosage increases (0.04–0.1 g/L), the number of available adsorption sites exceeds the ion concentration, thereby lowering the calculated adsorption capacity per unit mass [23-25]. Additionally, at elevated dosages, particle aggregation may occur, which reduces the effective surface area accessible for Pb(II) uptake and further decreases q_e. The optimal dosage for Pb(II) removal was determined to be 0.02 g under the studied conditions, which was subsequently employed in all experiments.

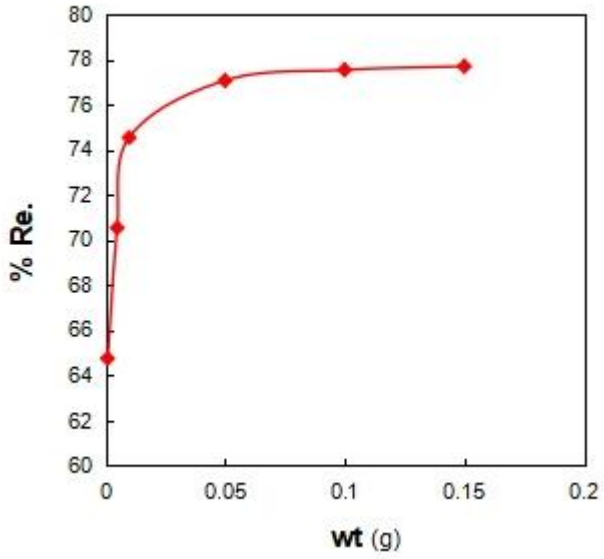

Figure 6. The effect of weight adsorbate on Pb adsorption (Co = 200 mg/l, 60 min, pH= 7).

3.3. Adsorption kinetics

The adsorption behavior of Pb(II) ions on the CMC-AAC-co-HEAM hydrogel was investigated as a function of contact time in the range of 0–240 minutes, with an initial concentration of 100 ppm and an adsorbent dose of 0.02 g. To describe the adsorption kinetics, the experimental data were fitted to the pseudo-first-order and pseudo-second-order models. The general expressions for the kinetic models are as follows:

Pseudo first order model [26-28]:

$$\ln(q_e - q_t) = \ln q_e - k_1 t \quad (1)$$

Pseudo second order model:

$$\frac{t}{q_t} = \frac{1}{k_2 q_e^2} + \frac{1}{q_e} t \quad (2)$$

The pseudo-first-order model yielded a correlation coefficient of R^2=0.8582 and a calculated equilibrium capacity (q_e=9.90mg g^{-1}), which significantly deviated from the experimental value (q_e≈40mg g^{-1}). In contrast, the pseudo-second-order model demonstrated an excellent fit, with a correlation coefficient of R^2=0.9997, and a calculated equilibrium capacity of q_e=40.32mg g^{-1}, which closely matched the experimental data. Furthermore, the initial adsorption rate (h_0) was determined to be 10.65 mg g^{-1} min^{-1}, reflecting the rapid uptake of Pb(II) during the early stages of the process (refer to **Table 1**). These findings confirm that the adsorption kinetics of Pb(II) on the CMC-AAC-co-HEAM surface follow the pseudo-second-order model, indicating that chemisorption is the dominant mechanism. This suggests that the interaction involves valence forces through electron sharing or exchange between Pb(II) ions and the functional groups (–COOH, –OH) of the hydrogel matrix [29].

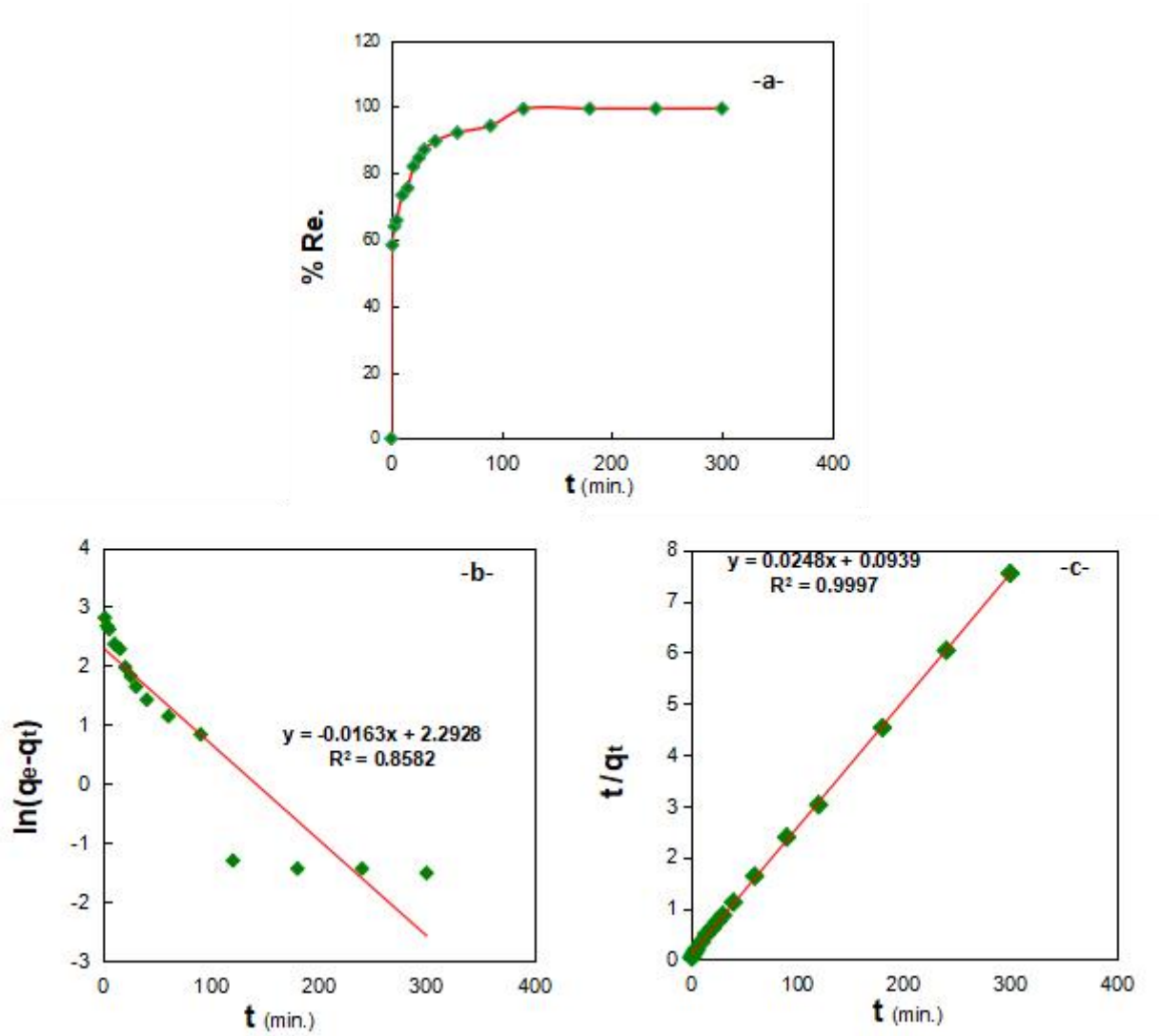

Figure 7. Kinetics graphs models and the removal and: (a) adsorption acapacity (b) pseudo first order (c) pseudo second order. (0.02 g, Pb: 10 mL and 100 mg/L)

Table 2. kinetic parameter of Pb on CMC-AAC-co-HEAM hydrogel using two model

Model	Parameter	Value	Units
Pseudo-First-Order (PFO)	$q_{e\ (calc)}$	9.90	mg g^{-1}
	k_1	0.0163	min^{-1}
	R^2	0.8582	–
Pseudo-Second-Order (PSO)	$q_{e(calc)}$	40.32	mg g^{-1}
	k_2	0.00655	g mg^{-1} min^{-1}
	$h_o=k_2q_e^2$	10.65	mg g^{-1} min^{-1}
	R^2	0.9997	–
Experiment	$q_{e(exp)}$	≈40	mg g^{-1}

3.4. Effect of pH

The pH of the solution plays a crucial role in controlling the adsorption efficiency of Pb(II) ions onto the CMC-AAC-co-HEAM hydrogel, as illustrated in **Figure 7**. The results revealed a clear enhancement in Pb(II) uptake with increasing pH. At pH 2.0, the equilibrium adsorption capacity (Q_e) was 35.92 mg/g, which increased steadily to 37.07 mg/g at pH 4.0, 39.30 mg/g at pH 6.0, and reached a maximum of 39.63 mg/g at pH 7.0. A further increase to pH 8.0 yielded a similar value (39.80 mg/g), indicating a plateau in adsorption capacity. The lower adsorption at acidic pH values can be attributed to the protonation of carboxyl and hydroxyl groups on the hydrogel surface, resulting in electrostatic repulsion between Pb(II) ions and the positively charged hydrogel matrix [30-32]. As the pH increased, deprotonation of these groups occurred, generating negatively charged sites that facilitated electrostatic attraction and complexation with Pb(II). Beyond pH 7.0, no significant increase in adsorption was observed, suggesting near-saturation of available sites. Thus, pH 7.0 was identified as the optimal condition for Pb(II) removal.

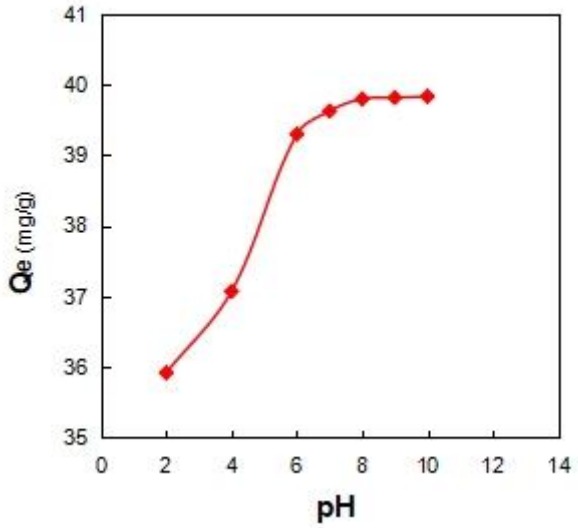

Figure 8. effects of pH on Pb adsorption (25ºC, 180 min, 0.02 wt).

3.5. Effect of salt (Ionic strength)

The influence of competing ions on Pb(II) adsorption by the CMC-AAC-co-HEAM hydrogel was evaluated using NaCl, KCl, and $CaCO_3$ electrolytes at different concentrations (**Figure 8**). The results revealed that increasing ionic strength reduced the adsorption capacity (Q_e) of the hydrogel for Pb(II). In the absence of salts, the hydrogel exhibited maximum adsorption capacities of 39.75, 39.66, and 39.60 mg/g for NaCl, KCl, and $CaCO_3$ systems, respectively. However, when the salt concentration reached 0.01 M, Q_e decreased to 34.99 mg/g for NaCl, 34.59 mg/g for KCl, and 34.07 mg/g for $CaCO_3$. This decline in adsorption efficiency can be attributed to the competition between Pb(II) ions and the introduced cations (Na^+, K^+, Ca^{2+}) for the active adsorption sites. The stronger suppression observed in the presence of Ca^{2+} ions compared with monovalent cations (Na^+, K^+) is due to its higher charge density, which enhances its affinity for negatively charged sites on the hydrogel [33]. These findings confirm that the adsorption of Pb(II) onto the hydrogel occurs primarily through electrostatic attraction and ion-exchange interactions, both of which are sensitive to ionic strength.

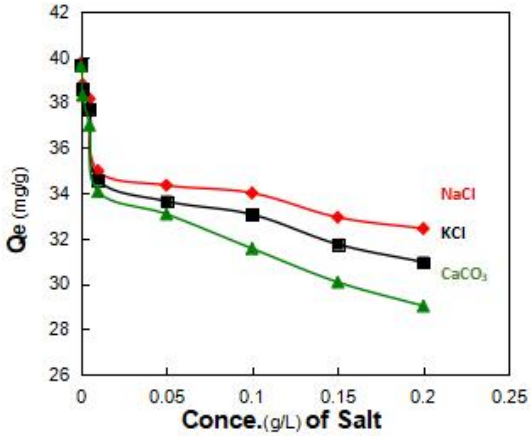

Figure 9. Effect of different electrolyte types (NaCl, KCl, and $CaCO_3$) at various concentrations on the adsorption capacity (Q_e) of Pb(II) ions onto CMC-AAC-co-HEAM hydrogel

3.6. Effect of temperature and thermodynamic analysis

The thermodynamic parameters obtained for the adsorption of Pb(II) ions onto CMC-AAC-co-HEAM hydrogel provide valuable insights into the mechanism of the process (**Figure 9**, **Table 2**). The negative Gibbs free energy (ΔG = –7.02 kJ/mol) indicates that the adsorption is spontaneous and thermodynamically feasible under the studied conditions. The positive enthalpy value (ΔH = +2.49 kJ/mol) confirms that the process is endothermic, implying that higher temperatures favor Pb(II) ion uptake due to enhanced mobility and diffusion through the hydrogel network. In addition, the positive entropy change (ΔS = +32.46 J/mol·K) suggests an increase in randomness at the solid–liquid interface, which may be attributed to the release of water molecules previously bound to active sites and the rearrangement of functional groups during Pb(II) binding. The equilibrium constant (K ≈ 7.14) further supports the strong affinity of the hydrogel towards Pb(II) ions. Overall, the thermodynamic evaluation confirms that the adsorption of Pb(II) onto the CMC-AAC-co-HEAM hydrogel is a spontaneous, feasible, and endothermic process, with improved performance at elevated temperatures [34,35].

Table 3. Thermodynamic parameters (ΔG, ΔH, and ΔS) for the adsorption of Pb(II) ions onto CMC-AAC-co-HEAM hydrogel at different temperatures.

ΔH(kJ/mol.)	ΔG(kJ/mol.)	ΔS(J/K.mol.)	(K)
2.490	-7.021	32.460	7.141

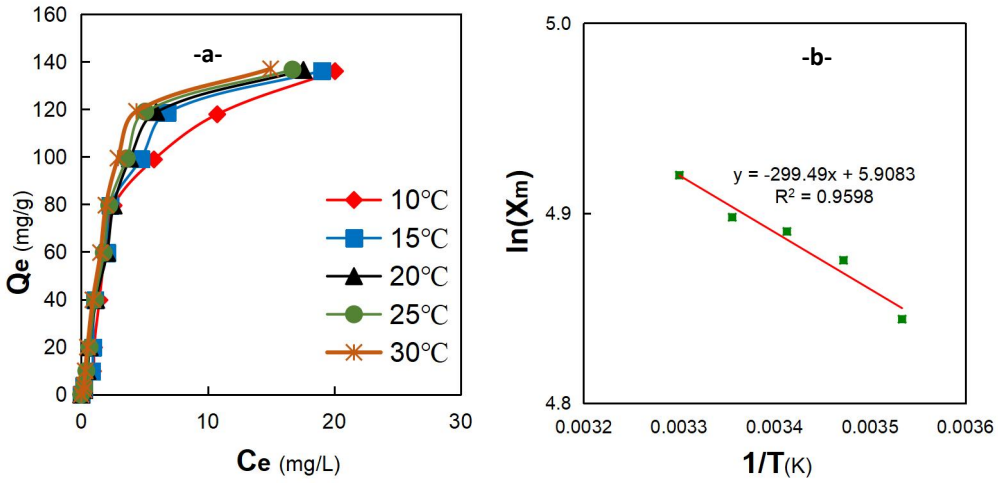

Figure 10. (a) Effect of temperature, (b) Van't Hoff plots for of Pb adsorption onto (CMC-AAC-co-HEAM) surface

3.7. Adsorption isotherm

The equilibrium adsorption data of Pb(II) ions onto the CMC-AAC-co-HEAM hydrogel were analyzed using Langmuir, Freundlich, and Temkin models (**Figure 10**) , and the corresponding constants are summarized in **Table 3**.

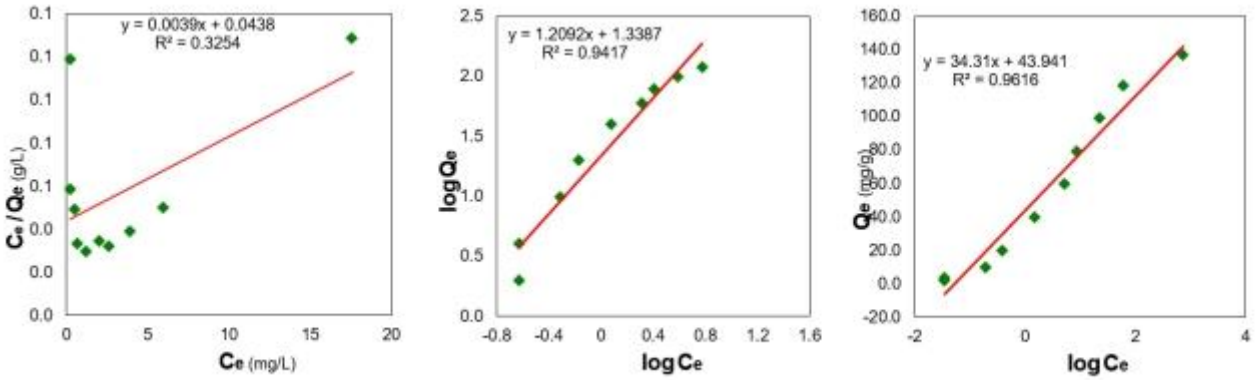

Figure 11. Adsorption isotherm plots of Pb(II) ions onto CMC-AAC-co-HEAM hydrogel fitted with Langmuir, Freundlich, and Temkin models.

Table 4. Adsorption isotherm constants of Pb(II) ions onto CMC-AAC-co-HEAM hydrogel according to Langmuir, Freundlich, and Temkin models.

Model	Slope	Intercept	R^2	q_m (mg/g)	K_L (L/mg)	R_L at Co=200	n	Kf	B (mg/g)	KT	b Temkin (J/mol)
Langmuir	0.0039	0.0438	0.3254	254.7115	0.0896	0.0529					
Freundlich	0.9851	1.3047	0.8753				1.0151	20.1679			
Temkin	34.3097	43.9412	0.9616						34.3097	3.5992	72.212

The Langmuir isotherm yielded a maximum monolayer adsorption capacity (q_m) of 254.71 mg/g with a Langmuir constant (K_L) of 0.0896 L/mg. The separation factor (R_L = 0.0529 at Co = 200 mg/L) falls between 0 and 1, confirming that the adsorption of Pb(II) onto the hydrogel is favorable. However, the relatively low correlation coefficient (R^2 = 0.3254) indicates that the Langmuir model does not adequately fit the experimental data, suggesting that Pb(II) adsorption does not occur strictly as a uniform monolayer process [36-38]. The Freundlich model provided a better correlation with the experimental data (R^2 = 0.8753) compared to Langmuir. The Freundlich constants (K_F = 20.17 and n = 1.015) indicate that the adsorption process is favorable (n > 1) and occurs on a heterogeneous surface with sites of varied affinities. The closeness of n to unity suggests nearly linear adsorption behavior, where the hydrogel surface accommodates Pb(II) ions without significant saturation at the studied concentrations [39,40]. The Temkin model showed the best agreement with the experimental data (R^2 = 0.9616), indicating that it is the most suitable isotherm to describe the adsorption mechanism of Pb(II) onto CMC-AAC-co-HEAM hydrogel. The Temkin binding constant (K_T = 3.599) and the Temkin constant (B = 34.31 mg/g) confirm that adsorption is influenced by adsorbate–adsorbent interactions. The calculated interaction parameter (b = 72.21 J/mol) implies moderate bonding energy between Pb(II) ions and the hydrogel functional groups, consistent with a chemisorption process involving carboxyl and hydroxyl groups. Overall, the results demonstrate that Pb(II) adsorption onto the CMC-AAC-co-HEAM hydrogel is best described by the Temkin isotherm, followed by Freundlich, while Langmuir provides the weakest fit. This indicates that adsorption occurs on a heterogeneous surface with significant adsorbate–adsorbent interactions rather than through ideal monolayer coverage. [4,5,41,42]

4. Conclusions

The CMC-AAC-co-HEAM hydrogel was successfully synthesized and characterized, showing porous morphology, abundant carboxyl and hydroxyl groups, and thermal stability up to ~200 °C. The hydrogel achieved a maximum Pb(II) uptake of ~39.8 mg/g under optimal conditions (0.02 g dosage, pH 7), with adsorption efficiency decreasing in the presence of competing ions, particularly Ca^{2+}. Kinetic studies confirmed a pseudo-second-order mechanism, while thermodynamic analysis indicated that adsorption was spontaneous, endothermic, and entropy-driven. Among the equilibrium models, the Temkin isotherm best described the process, highlighting heterogeneous adsorption with moderate interaction energies. These findings demonstrate that CMC-AAC-co-HEAM hydrogel is a cost-effective and environmentally sustainable adsorbent for Pb(II) removal from aqueous solutions. Further research is required to study the reusability of hydrogel for analysis of its better performance.

Conflict of interest

The authors declare no conflict of interest

References

1. Largitte L; Pasquier R. A review of the kinetics adsorption models and their application to the adsorption of lead by an activated carbon. Chemical engineering research and design. 2016;109:495-504
2. Li Y-H; Wang S; Wei J; Zhang X; Xu C; Luan Z; Wu D; Wei B. Lead adsorption on carbon nanotubes. Chemical physics letters. 2002;357(3-4):263-266
3. Neamah Thamer A; S. Alwan A; A. Alwan N; Jasim LS; Batool M. Adsorptive removal of chromium (Cr (III)) and lead (Pb (II)) ions from water using crosslinked polyvinyl alcohol-acrylamide P (VA-AAm) hydrogel. International Journal of Environmental Analytical Chemistry. 2025:1-26
4. Al-Hasan HA; Th. AL- Suraify SM; Othman MA-M; Jasim LS; Batool M. Activated Nano-Carbon from Natural Sources for Water Treatment: A Comprehensive Review. Journal of Nanostructures. 2025;15(3):1443-1456.10.22052/jns.2025.03.058
5. Khudhair MM; Safaa Abdulkadhim A; Layth SJ; Maryam B. Efficient adsorption of congo red dye from aqueous solution using MWCNT/Chitosan-g-Poly (acrylic acid–crotonic acid) composite. Applied Chemical Engineering. 2025;8(3):ACE-5729.10.59429/ace.v8i3.5729
6. in L; Bai R. Mechanisms of lead adsorption on chitosan/PVA hydrogel beads. Langmuir. 2002;18(25):9765-9770
7. Chai WS; Cheun JY; Kumar PS; Mubashir M; Majeed Z; Banat F; Ho S-H; Show PL. A review on conventional and novel materials towards heavy metal adsorption in wastewater treatment application. Journal of Cleaner Production. 2021;296:126589
8. Demirbas A. Heavy metal adsorption onto agro-based waste materials: a review. Journal of hazardous materials. 2008;157(2-3):220-229
9. Hmood NA; Othman MAM; Ali MM. Transcription factor 7-like 2 gene polymorphisms rs7903146associationwith type 2 diabetic polycystic ovarian syndrome women of Iraqi Population. Annals of Tropical Medicine and Public Health. 2019;22(12).10.36295/ASRO.2019.221216
10. AlSaadi EK; Darweesh MA; Al Jawadi HF; Othman MAM. Demographic Characteristics, Clinical Features, Laboratory, and Radiological Findings in Children Admitted to COVID19 Center in Amara City, Misan Province, Iraq. Journal of Medicinal and Chemical Sciences. 2023;6(1):34-43.10.26655/JMCHEMSCI.2023.1.5
11. Imran M; Anwar K; Akram M; Shah GM; Ahmad I; Samad Shah N; Khan ZUH; Rashid MI; Akhtar MN; Ahmad S. Biosorption of Pb (II) from contaminated water onto Moringa oleifera biomass: kinetics and equilibrium studies. International Journal of Phytoremediation. 2019;21(8):777-789
12. Mutashar MO; Shahad RF; Jasim IS; Batool M. Removal of Pb (II) Ions from Water by Adsorption on Sodium Alginate-g-poly (Acrylic acid-co-Itaconic acid)/Titanium Dioxide [SA-gp (AA-IA)/TiO2] Hydrogel Nanocomposite. Journal of Nanostructures. 2025;15(3):983-996
13. Alnasery H; Naseri A; Jasim LS; Sajedi-Amin S. Synthesis, characterization, and adsorption capacity of sodium alginate poly grafted (fumaric acid-co-polyacrylic acid)/graphene oxide hydrogel as adsorbent for Cr (VI) and Pb (II) removal. Journal of the Iranian Chemical Society. 2024:1-13
14. Kaur M; Kumari S; Sharma P. Removal of Pb (II) from aqueous solution using nanoadsorbent of Oryza sativa husk: Isotherm, kinetic and thermodynamic studies. Biotechnology Reports. 2020;25:e00410
15. Alnasery H; Naseri A; Jasim LS; Sajedi-Amin S. Synthesis, characterization, and adsorption capacity of sodium alginate poly grafted (fumaric acid-co-polyacrylic acid)/graphene oxide hydrogel as adsorbent for Cr (VI) and Pb (II) removal. Journal of the Iranian Chemical Society. 2024;21(7):1915-1927.10.1007/s13738-024-03037-3

16. Alzayd AAM; Zghair AN; Essa AM; Jawad AS; Abed MJ; Batool M; Jasim LS. Isotherm and Thermodynamic Analysis of Azur C Dye Adsorption on GO/P (CMC-Co-Am) Nanocomposite. Journal of Nanostructures. 2024;14(3):845-856
17. Batool M; Haider MN; Javed T. Applications of spectroscopic techniques for characterization of polymer nanocomposite: A review. Journal of Inorganic and Organometallic Polymers and Materials. 2022;32(12):4478-4503
18. Ali MM; Mhaibes RM; Othman MAM; Lahhob QR; Qasim MJ. Association between triglyceride-glucose index and risk of chronic kidney disease: a systematic review and meta-analysis. Journal of Nephropharmacology. 2024;13(2).10.34172/npj.2024.12692
19. Zghair AN; Al-Khateeb ZT; Jasim LS; Batool M. Synthesis, characterization and adsorption properties of azo-functionalized polymeric hydrogels for R6G dye removal from water. Applied Chemical Engineering. 2025;8(1).10.59429/ace.v8i1.5604
20. Mojar Alshamusi QK; Hameed KAA; Taher AM; Batool M; Jasim LS. Efficiency of Chitosan-Grafted Poly (Carboxymethyl Cellulose-Co-Acrylamide) Nano Hydrogel for Cadmium (II) Removal: Batch Adsorption Study. Journal of Nanostructures. 2024;14(4):1122-1133.10.22052/JNS.2024.04.013
21. Dong S; Li Y; Zhu K; Wang C; Zhai S. Advances in structure designing and function tailoring strategy toward alginate-based hydrogels for efficient water remediation: A review. International Journal of Biological Macromolecules. 2025:140801
22. Majeed HJ; Idrees TJ; Mahdi MA; Abed MJ; Batool M; Yousefi SR; Thumma A; Jasim LS. Synthesis and application of novel sodium carboxy methyl cellulose-g-poly acrylic acid carbon dots hydrogel nanocomposite (NaCMC-g-PAAc/CDs) for adsorptive removal of malachite green dye. Desalination and Water Treatment. 2024;320:100822
23. Saadallah K; AD C; Djedid M; Batool M; Benalia M; Saadallah S; Hamamda S. Potential of the Algerian pine tree bark for the adsorptive removal of methylene blue dye: Kinetics, isotherm and mechanism study. Journal of Dispersion Science and Technology. 2024:1-19
24. Taher AM; Jasim LS; Mehmood Z; Zawar MD; Haider MN; Batool M. Applications of Nano Composites for Heavy Metal Removal from Water by Adsorption: Mini Review. Journal of Nanostructures. 2024;14(4):1239-1251.10.22052/JNS.2024.04.023
25. Zeeshan M; Javed T; Kumari C; Thumma A; Wasim M; Taj MB; Sharma I; Haider MN; Batool M. Investigating the Interactions between Dyes and Porous/Composite Materials: A Comprehensive Study. Sustainable Chemistry for the Environment. 2025:100217.https://doi.org/10.1016/j.scenv.2025.100217
26. Shah A; Arjunan A; Thumma A; Zakharova J; Bolarinwa T; Devi S; Batool M. Adsorptive removal of arsenic from drinking water using KOH-modified sewage sludge-derived biochar. Cleaner Water. 2024;2:100022
27. Shah A; Zakharova J; Batool M; Coley MP; Arjunan A; Hawkins AJ; Bolarinwa T; Devi S; Thumma A; Williams C. Removal of cadmium and zinc from water using sewage sludge-derived biochar. Sustainable Chemistry for the Environment. 2024;6:100118
28. Gao C; Wang X-L; An Q-D; Xiao Z-Y; Zhai S-R. Synergistic preparation of modified alginate aerogel with melamine/chitosan for efficiently selective adsorption of lead ions. Carbohydrate polymers. 2021;256:117564
29. Yang C; Yang H-R; Li S-S; An Q-D; Zhai S-R; Xiao Z-Y. Rationally designed carboxymethylcellulose-based sorbents crosslinked by targeted ions for static and dynamic capture of heavy metals: Easy recovery and affinity mechanism. Journal of Colloid and Interface Science. 2022;625:651-663
30. Javed T; Kausar F; Zawar MD; Khalid N; Thumma A; Ismail A; Alzaidy AH; Abed MJ; Jasim LS; Taj MB; Tirth V; Haider MN. Investigating the adsorption potential of coconut coir as an economical adsorbent for decontamination of lanthanum ion from aqueous solution. Journal of Dispersion Science and Technology. 2024.10.1080/01932691.2024.2431093
31. Urooj H; Javed T; Taj MB; Nouman Haider M. Adsorption of crystal violet dye from wastewater on Phyllanthus emblica fruit (PEF) powder: kinetic and thermodynamic. International Journal of Environmental Analytical Chemistry. 2024;104(19):7474-7499
32. Argun ME; Dursun S; Ozdemir C; Karatas M. Heavy metal adsorption by modified oak sawdust: Thermodynamics and kinetics. Journal of hazardous materials. 2007;141(1):77-85
33. Jamel HO; Jasim MH; Mahdi MA; Ganduh SH; Batool M; Jasim LS; Haider MN. Adsorption of Rhodamine B dye from solution using 3-((1-(4-((1H-benzo[d]imidazol-2-yl)amino)phenyl)ethylidene)amino)phenol (BIAPEHB)/ P(AA-co-AM) composite. Desalination and Water Treatment. 2025;321.10.1016/j.dwt.2025.101019
34. Bukhari A; Javed T; Haider MN. Adsorptive exclusion of crystal violet dye from wastewater by using fish scales as an adsorbent. Journal of Dispersion Science and Technology. 2023;44(11):2081-2092
35. Imran MS; Javed T; Areej I; Haider MN. Sequestration of crystal violet dye from wastewater using low-cost coconut husk as a potential adsorbent. Water Science and Technology. 2022;85(8):2295-2317
36. Celis R; Hermosin MC; Cornejo J. Heavy metal adsorption by functionalized clays. Environmental science & technology. 2000;34(21):4593-4599
37. González A; Pokrovsky O. Metal adsorption on mosses: toward a universal adsorption model. Journal of colloid and interface science. 2014;415:169-178

38. Jiang C; Wang X; Wang G; Hao C; Li X; Li T. Adsorption performance of a polysaccharide composite hydrogel based on crosslinked glucan/chitosan for heavy metal ions. Composites Part B: Engineering. 2019;169:45-54
39. Vieira RM; Vilela PB; Becegato VA; Paulino AT. Chitosan-based hydrogel and chitosan/acid-activated montmorillonite composite hydrogel for the adsorption and removal of Pb+ 2 and Ni+ 2 ions accommodated in aqueous solutions. Journal of Environmental Chemical Engineering. 2018;6(2):2713-2723
40. Godiya CB; Cheng X; Li D; Chen Z; Lu X. Carboxymethyl cellulose/polyacrylamide composite hydrogel for cascaded treatment/reuse of heavy metal ions in wastewater. Journal of hazardous materials. 2019;364:28-38
41. Arshad R; Javed T; Thumma A. Exploring the efficiency of sodium alginate beads and Cedrus deodara sawdust for adsorptive removal of crystal violet dye. Journal of Dispersion Science and Technology. 2024;45(12):2330-2343
42. Lin Z; Yang Y; Liang Z; Zeng L; Zhang A. Preparation of chitosan/calcium alginate/bentonite composite hydrogel and its heavy metal ions adsorption properties. Polymers. 2021;13(11):1891
43. Al-Suraify SMT, Hussien LB. RETRACTED ARTICLE: Synthesis and characterization of new compounds derived from 1H-indol-5-ylamine (Applied Nanoscience, (2023), 13, 3, (2083-2092), 10.1007/s13204-021-02080-3). Applied Nanoscience (Switzerland). 2024;14(4):719.
44. Al-Suraify SMT, Hussien LB. Synthesis and characterization of new compounds derived from 1H-indol-5-ylamine. Applied Nanoscience (Switzerland). 2023;13(3):2083-92.
45. Hmood NA, Othman MAM, Ali MM. Transcription factor 7-like 2 gene polymorphisms rs7903146associationwith type 2 diabetic polycystic ovarian syndrome women of Iraqi Population. Annals of Tropical Medicine and Public Health. 2019;22(12).
46. Karim AN, Jasim LS. Synthesis and characterization of poly (CH/AA-co-AM) composite: Adsorption and thermodynamic studies of benzocaine on from aqueous solutions. International Journal of Drug Delivery Technology. 2019;9(4):558-62.
47. Al-Suraify SMT. Synthesis and characterization of novel compounds derived from 6-methyl-2,6 dihydro[1,2,4-triazino[4,3-b] indazol-3(4h)-one. International Journal of Pharmaceutical Research. 2020;12:1504-17.